EasyChair Preprint

№ 13450

Seismic Performance Verification of Rapid-Disassembly Carbon-Minimized Dismantle Connection

Hyeongjin Choi, Sanghoon Kim, Youngju Kim, Jaehyeok Doh and Jaehoon Bae

May 29, 2024

Seismic Performance Verification of Rapid-Disassembly Carbon-Minimized Dismantle connection

Hyeongjin Choi[1] and Sanghoon Kim[2] and Youngju Kim[3] and Jaehyeok Doh[4] and Jaehoon Bae[5*[0000-0001-8940-5255]]

1 Chonnam National University, Department of Architecture Design 50 Daehak-ro, Yeosu, Jeonnam 59626, Republic of Korea
2 Chonnam National University, Department of Mechanical Design Engineering 50 Daehak-ro, Yeosu, Jeonnam 59626, Republic of Korea
3 Korea Institute of Structural Engineering & Consulting, Busan, Republic of Korea
4 Gyeongsang National University, School of Aerospace Engineering, Jinju, Gyeongsang-nam-do 52828, Republic of Korea
5 Chonnam National University, Department of Architecture Design 50 Daehak-ro, Yeosu, Jeonnam 59626, Republic of Korea
skycity-bjh@jnu.ac.kr

Abstract. The concept of "carbon neutral, easy to dismantle connection" was introduced to meet the global demand for sustainable and environmentally friendly construction. This innovative design utilizes the 3R principles: reduce, recycle, and reuse. This study introduces a new connection with a prequalified shape that can be quickly disassembled. The main feature of the carbon-neutral dismountable joint is that it can be easily constructed using a sliding mechanism and quickly assembled using bolts without welding. This shortens the construction time and facilitates the dismantling of the beam-column structure, making it highly efficient in terms of time and labor. In addition, this connection design efficiently distributes shear stress across the flanges and webs of the structure, thereby improving shear resistance. This feature ensures that the integrity and strength of the connection is maintained under seismic loads without compromising internal strength. Notably, this connection requires less steel for construction, making it a more economical option than traditional methods. This reduction in material usage is in line with the principles of sustainability and carbon neutrality. Extensive experimental and numerical studies have been conducted to verify the effectiveness of the CNDCs. This study focused on the analysis of the cyclic response of the connections under seismic conditions. The result of this study confirmed that the connection maintained its strength and integrity throughout the seismic simulations.

Keywords: Beam–Column Connection, Steel Structure, Modular Structure, Carbon Neutrality Design.

1 Introduction

Steel structures are widely used in construction. They are known for their cost-effectiveness, rapid construction, and sustainability [1]. While the melting and processing of metallurgically recyclable steel is energy and CO2 intensive [2], the reuse of steel in structural components can reduce environmental and economic costs with minimal processing, such as cutting. Steel framing allows structural components to be reused, bypassing the need for recycling [3]. This approach minimizes waste and carbon emissions through efficient prefabrication and on-site assembly [4-5]. Therefore, easy-to-assemble and disassemble connections further enhance member reuse. This promotes sustainability in construction practices.

The Northridge (1994) and Kobe (1995) earthquakes caused the buckling of beam-column connections, which led to numerous studies to improve the performance of steel moment frame connections. The SAC joint venture in the United States focused on validating various connection details [6-7].

The effectiveness of beam-column connections is critical to the seismic and mechanical performance of steel structures, affecting bending moments, shear forces, and axial load transfer [8]. Box sections are preferred in seismic regions due to their high biaxial flexural and torsional stiffness, ductility, and post-buckling capacity, and are commonly used as compression members in steel frames [9-10]. In addition, box columns can be filled with concrete; a concrete-filled tube (CFT) is widely used. It can increase the strength, stiffness, and fire resistance [11-12].

Extensive research has been developed on connections using box columns and H-beams, and various moment frame connections have been developed to transfer stresses from the beam flanges to the columns when loading occurs. These connections are categorized based on the position of the load-transferring components relative to the column: 1) extending into the column or 2) surrounding the column.

The former types, which are integrated into columns, involve modifying boxed steel pipes to insert diaphragms and then re-welding them. Azizinamini et al. and Elremaily conducted studies on connections between CFT columns and H-beams within rigid frames [13-14]. Mohammadi et al. introduced a concept involving a separated through-diaphragm with vertical plates [15-16]. Cao et al. developed a new type of connection that includes a bottom-through-diaphragm and a top-ring [17]. On the other hand, the latter type, known as external membrane type, employs horizontal and cover plates for load transfer. Shin et al. and Ghobadi identified and addressed the limitations of traditional external diaphragms, especially regarding weld quality, through the use of reinforced T-stub connections [18-19]. Zhang et al. introduced a new modular joint that utilizes field-bolted connections [20]. Lastly, Rezaeina et al. and Yang et al. evaluated and detailed the AISC 358-10 certified ConXL connections [6,21,22].

A distinctive vertical “kink” in stress distributions and load paths has been identified in beam assemblies, particularly near columns and constrained beam webs [23], which is shown in Figure 1. Based on Lee et al.’s truss analogy, we propose

the TZcon connection module. This design uses a shear bolt connection complemented by a vertical rib plate to effectively address the bending and shear forces near the beam flange. Unlike typical designs, the TZcon module does not directly connect the center of the column to the beam web. Instead, load transfer efficiency is improved by using a cover over the flange section. The primary stress within the H-beam connected to the column at the column–beam connection of the central part of the web shows minimal stress transfer and occurs mainly near the flange.

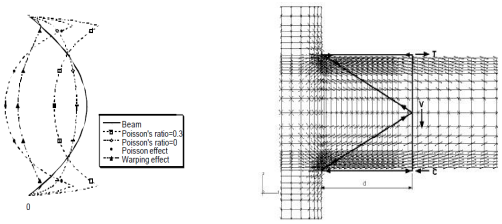

Fig. 1. Stress contributions of boundary effects near the support of the rectangular beam.

Based on the truss-analogy, this study proposes a connection of box columns and H-beams that does not constrain the center of the web. The geometry and mechanical properties were verified using ABAQUS software [24] to achieve the ideal joint and tested at full scale. Despite fabrication errors resulting in tolerance between the TZcon at a test at full scale, the seismic performance meets the required standards. The TZcon joint module offers various advantages, including rapid construction, worker safety, component reuse, improved seismic performance, material savings, and environmental friendliness. Prefabricated in the shop, this module ensures precise weld quality, improves transportability to the site, and is smaller in volume than traditional outer diaphragm forms. The CNDC system can also be termed as a "Direct Reuse Circular Economy Approach", which can be an option to significantly reduce the embodied carbon considering the whole life cycle for the sustainability of construction [25-26].

2 Introduction of CNDC

2.1 Specification of TZcon

The general configuration of the CNDC connection system using the proposed TZcon and detail is shown in Figure 2. The general connection is a combination of bolted and welded connections where all components, including the TZcon and H-beam, are prefabricated in a shop and assembled on-site using bolts. The main components of the TZcon consist of trapezoidal horizontal segments at the top and bottom flanges of the H-beam, corner segments at the top and bottom, and vertical segments that transfer loads to the column component located in the web. In addition, a shear tab is incorporated at the center of the column.

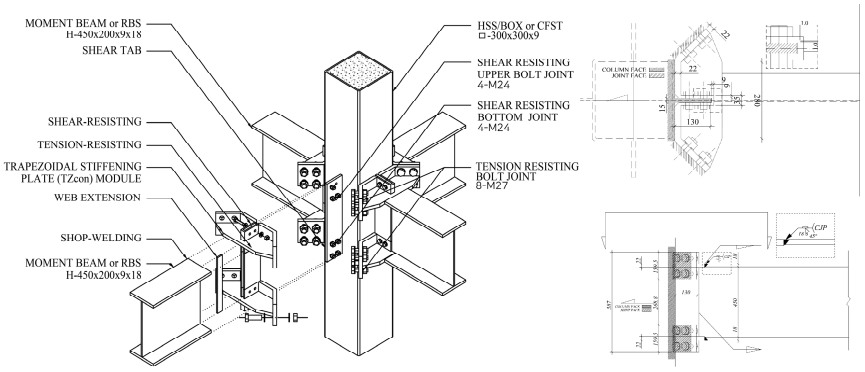

Fig. 2. Specification of TZcon connection.

2.2 Numerical verification

Figure 3 shows the Von Mises stress distribution at the displacement load of 4%. The concentration of stress is observed to be high near the flange of the beam. Also, by applying increasing cyclic displacement loads, stresses were generated near the shear tab of the columns. This is because the corner segments at the top and bottom transferred the moment to the shear tabs of the column. However, this is a very small level of plastic area that can be ignored. Figure 4 shows the hysteresis curve of the FEM model. The area and stiffness of the curve for each cycle is ideal and show that the ductility capacity was sufficient.

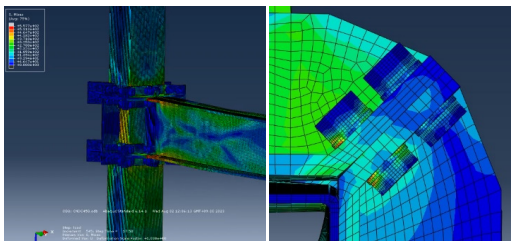

Fig. 3. Stress distribution.

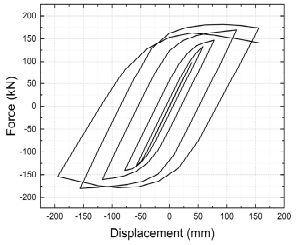

Fig. 4. Hysteresis response.

2.3 Assembly progress and details of joints

Figure 5 shows the assembly process. In the shop, beam members are made by welding TZcon and H-beam, and column members are made by welding shear tab and box column (Fig. 5a). The members are transported from the shop to the site, and the two members are inserted in a vertical sliding manner and joined with four M24 bolts (Fig. 5b). The CNDC system, which is connected in the same way, is fastened with a total of 16 M27 bolts, four on each side of the corner segment of TZcon and eight M24 bolts on the shear tab and vertical segment of TZcon per welded beam (fig. 5d). As shown in Figure 6, the structural prototype includes alternative column positions based on the presence or absence of the beam.

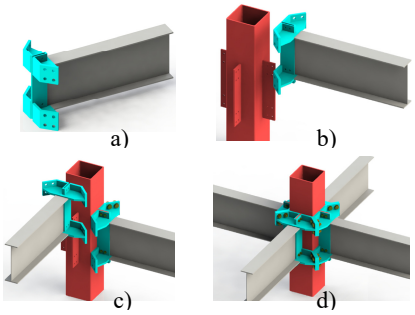

Fig. 5. Assembly process of connection.

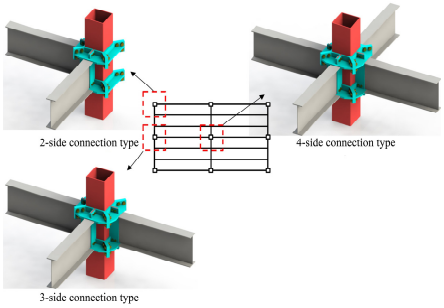

Fig. 6. TZcon alternative design for column positions.

3 Experimental study

3.1 Dimensions and material properties of specimens

In this study, four joint specimens (CNDC-450, CNDC-500, CNDC-500R, and CNDC-500W) were fabricated, along with a comparative specimen (EXT-450C). In addition, specimens were fabricated to evaluate the performance of the CNDC prototypes. CNDC-500W has a beam on one side. Specimens with shear tabs on all four sides were fabricated except for this variation. The distance between the load points from the column center was 3,500 mm. The steel beam was constructed using welded H-beams (SS275). To observe the moment resistance behavior of the joints, beams with depths of 450 mm and 500 mm were constructed based on the axis, and the specimens were named accordingly. For all specimens, square hollow sections of □-300 × 300 × 9 (SRT275) were used for the column, and the length of the column, including both ends with end plates, was 2,000 mm. The CNDC-500R specimen has an RBS cutout, and the RBS design was based on the work of Engelhardt et al [27]; the specifications are illustrated in Figure 7.

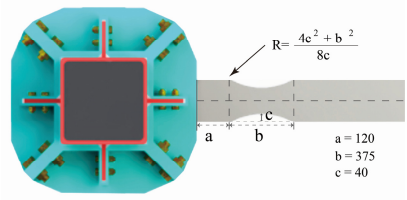

Fig. 7. Specification of RBS section.

To evaluate the material strengths of the box-shaped steel column, H-beam, and steel plate in the joints, tensile strength tests were performed on the specimens. The tensile tests were performed on the three specimens prepared for each experimental setup, and the obtained values were averaged. Table 1 confirms that all specifications were satisfied for each steel grade.

Table 1. Material properties of steel.

Components	Thickness (mm)	Steel grade	F_y (MPa)	F_u (MPa)	Elong. (%)	Yield ratio (%)
Column	Plate (t = 9 mm)	SRT 275	392.51	481.50	20.73	81.52
Beam, Stiffeners	Plate (t = 9 mm)		291.80	448.55	30.82	65.05
Beam, Diaphragm	Plate (t = 18 mm)	SS275	288.37	444.18	30.86	64.92
Shear tab	Plate (t = 15 mm)		275.89	433.83	31.53	63.59
Stiffeners	Plate (t = 22 mm)		281.44	451.43	30.65	62.34

3.3 Test setup

Figure 8 shows an overview of the test setup. The top and bottom of the column were hinged to a reaction wall, and the end of the beam was subjected to an actuator with a capacity of 3,000kN. To prevent out-of-plane deformation of the H-shaped steel during loading, lateral support jigs were installed at both ends of the applied load, and the displacement measurements were performed using a displacement gauge (wire gauge) installed under the beam at the center point. Loading was applied based on the multistage seismic loading protocol of SAC 2000 [7], and the displacement at the end of the beam was divided by the length from the beam end to the column center to calculate the story drift ratio (SDR) θ, as shown in Figure 9. Each test was terminated when the load at the beam end decreased by 85% of the maximum load.

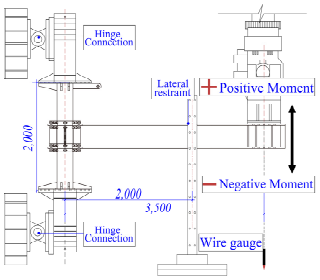

Fig. 8. Test setup diagram (unit: mm).

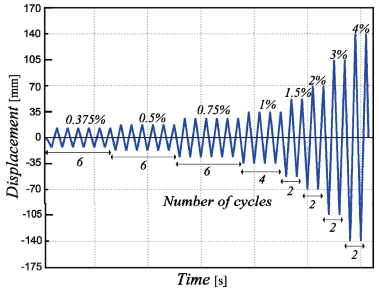

Fig. 9. SAC 2000 cyclic loading protocol.

4 Experimental results and discussion

4.1 Test phenomena and Failure mode

The final failure modes of the four full-size CNDC specimens are shown in Figure 10 (b), (c), (d), and (e). A summary of the test results is presented in Table 2. Specimen (b) CNDC-450 is used to illustrate the main observations. The entire

CNDC specimen failed at the weld where the plastic hinge abutted the joint and flange. The deformation was not prominent until θ = 0.02 rad. At θ = 0.03 rad, some paint peeling and bulging of the flange close to the joint were observed. At θ = 0.04 rad, the column face surrounded by the TZ con was buckled by the force, and a small crack appeared between the lower flange and the joint. At θ = 0.06 rad, the load was reduced due to the rapid increase in the deformation of the flange and increased cracking along the weld, resulting in fracture through the lower flange at two cycles, ending the experiment.

Fig. 10. Failure mode of test specimens.

(a)EXT-450C (6% drift: Top flg.) (b) CNDC-450 (6% drift: Bot. flg.) (c) CNDC-500 (5% drift: Top flg.) (d) CNDC-500R (5% drift: Top flg.) (e) CNDC-500W (6% drift: Bot. flg.)

Table 2. Summary of the test result.

Specimens	M^{+}_{max} (kN·M)	M^{-}_{max} (kN·M)	θ^{+}_{max} (%)	θ^{-}_{max} (%)	M^{+}_{max} / M_n	M^{-}_{max} / M_n
EXT-450C	462.4	-487.2	5.3	-5.1	0.87	0.91
CNDC-450	566.0	-586.5	6.1	-6.1	1.06	1.1
CNDC-500	609.6	-727.0	5.1	-5.1	1	1.19
CNDC-500R	569.9	-655.7	5.1	-6.1	0.93	1.07
CNDC-500W	582.9	-664.9	6.1	-6.1	0.95	1.09

4.2 Hysteresis behaviour

The moment–rotation curves of each specimen obtained experimentally are shown in Figure 11. The value of M_{max}/M_n was above 0.8 at 0.04 radian for all of the specimens before CNDC, and all of them had a rotation angle of more than 5% and excellent performance. However, unlike the EXT specimen, the hysteresis curve was not plump but pinched inward. As listed in Table 2, the maximum moment ratio (M_{max}/M_n) to the moment of plasticity is 1.19 for the CNDC-500 specimen and 0.93 for the CNDC-500R specimen, with a difference of 1.1–1.23 times that of the EXT-450 specimen.

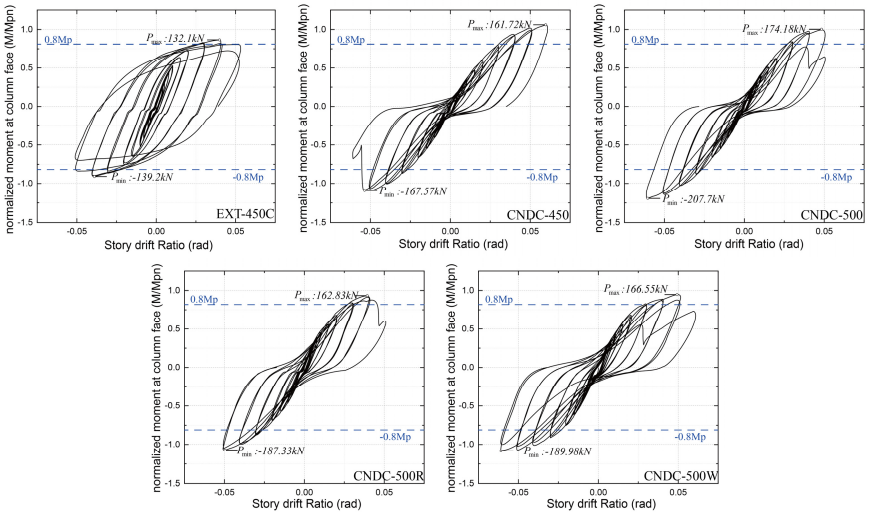

Fig. 11. Hysteresis responses for all models.

4.3 Skeleton curve and Initial stiffness degradation curve

Figure 12's skeleton curve shows elastic, elastic-plastic, and strength-declining stages. Most CNDC specimens, except EXT-450C, transition to the elastic-plastic stage between θ = 0.02 and 0.03 rad, shown by a slope decrease. indicating the joint entering the elastic–plastic stage. Despite a shorter elastic stage, CNDC specimens had higher ultimate strength than the comparison specimen. Figure 13 illustrates the graph of stiffness degradation for loading cycles. The y-axis represents the ratio of the stiffness of each loading stage to the initial average stiffness (K_1 = (K_{1+} + K_{1-})/2) expressed as the ratio of initial stiffness (K_i / K_1). The x-axis corresponds to the loading step. Stiffness degradation is most noticeable in the CNDC-450 specimen, whereas the EXT-450 specimen has the highest stiffness. The CNDC-450 specimen exhibited an approximately 18% larger stiffness compared to the initial stage, and the stiffness degradation rate of the EXT-450C specimen was generally higher than that of the other specimens.

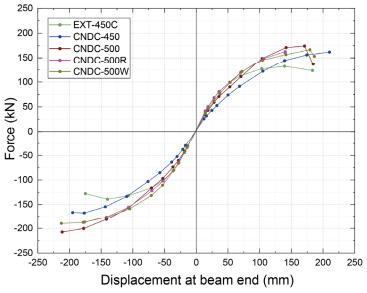

Fig. 12. Skeleton curve of all models.

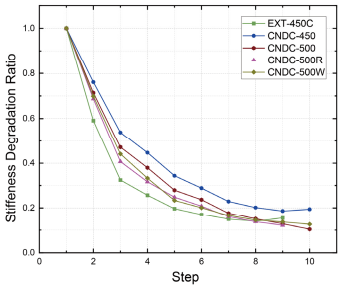

Fig. 13. Curve of Stiffness degradation.

4.4 Energy dissipation capacity

Utilizing energy dissipation, which is characterized by the area enclosed within the hysteresis loop of each cycle in the repeated loading process, allows the energy dissipation capability of the joint to be identified. Overall, the dissipation capacity of the CNDC specimen was about 64% of that of the comparison specimen (EXT-450) due to manufacturing errors (distance of 5–8 mm), leading to pinching phenomena. Figure 14 shows that CNDC-500W has the highest total energy dissipation capacity at 77.96 kN·M, whereas CNDC-500R has the lowest at 47.66 kN·M, and it reaches failure at 0.04 radians. However, the dissipation capacity for each displacement in Figure 15 shows that CNDC-450 has the lowest values.

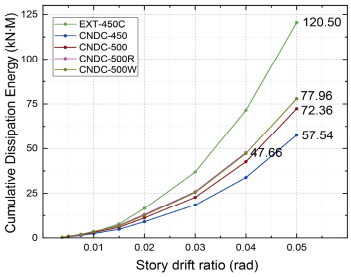

Fig. 14. Cumulative energy dissipation capacity.

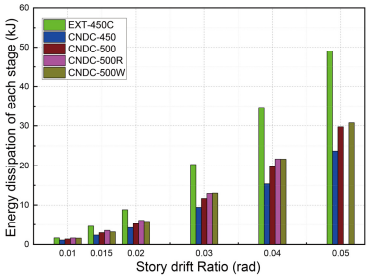

Fig. 15. Each stage of energy dissipation of joints (0.01rad – 0.05rad).

4.5 Stress and Strain Analysis

Figure 16 shows the strain curves of five full-scale specimens. The horizontal axis of the figure represents the measuring point of the gauge. CF1 and CF2 are located on the top left and right sides of the TZcon. BF1, BF2, BF3 and BF4 are located at the tops of the beam flanges, while BW1 and BW2 are the beam webs. Before θ = 0.01, the flange and web of the jointed beam were primarily in the elastic stage, with only measurement point BF1 reaching the yield point. At θ = 0.02, compared to the EXT-450C specimen, the beam flanges generally showed more localized strain than the web section. After θ = 0.04, for CNDC specimens with a beam depth of 500 mm, stress near the joint was minimal, whereas, at a depth of 450 mm, the stress was seemingly distributed around the joint.

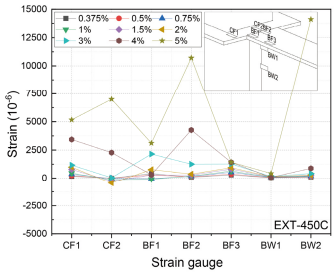

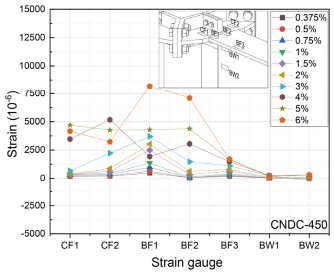

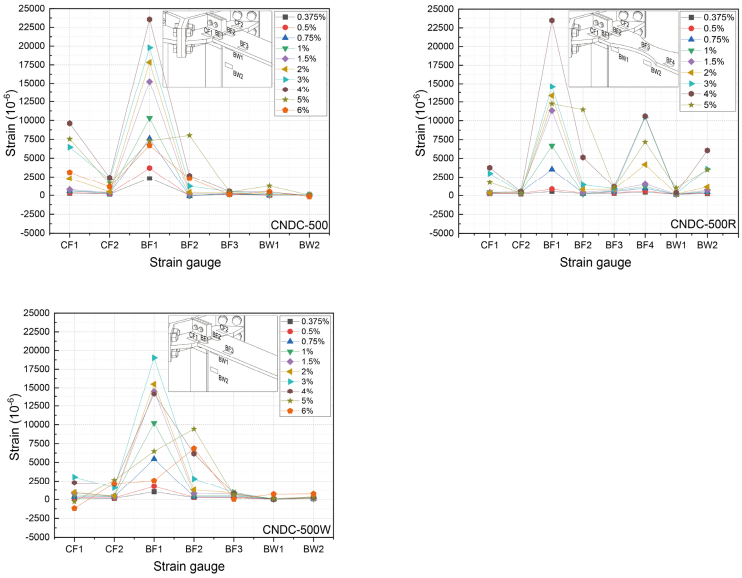

Fig. 16. Strain distributions of location.

5 Conclusions

In this paper, an innovative beam-column joint system using bolted modular joints of TZcon that can be dismantled to realize carbon neutrality is proposed, the seismic performance is verified by FEM analysis and full-scale experiments are conducted. The main conclusions are as follows.

1. The beam–column joints of the system were evaluated to realize the AISC/SAC seismic performance requirements; the plastic moment up to 0.04 radian in the positive-negative moment section was more than 80% that of the typical exterior diaphragm.
2. Due to an error in the production of the test specimen, the joint separation distance was 5-8 mm, and the test was conducted in a gap condition. As a result, excessive pinching occurred due to the opening and closing motion between the joint and the column, resulting in inferior performance compared to the control specimen in terms of energy dissipation.
3. The column element may have been weakly designed, which may have led to excessive deformation of the column or external deformation in the tensile cycle during the test, which may have influenced the occurrence of pinching phenomena.
4. It was experimentally verified that the CNDC system has sufficient stiffness and seismic performance. In the future, further theoretical studies and improvement of joint details using FEM analysis are needed to solve the cause of the pinching phenomenon.

6 Acknowledgements

This work was supported by the National Research Foundation of Korea (NRF) grant funded by the Korean government (MSIT) (No.2022R1C1C1003594).

References

1. The American Institute of Steel Construction (AISC), https://www.aisc.org/why-steel/ten-reasons-to-use-structural-steel/, last accessed 2024/03/21.
2. Kim, Jinsoo, Benjamin K. Sovacool, Morgan Bazilian, Steve Griffiths, Junghwan Lee, Minyoung Yang, and Jordy Lee. 2022. "Decarbonizing the Iron and Steel Industry: A Systematic Review of Sociotechnical Systems, Technological Innovations, and Policy Options." Energy Research & Social Science 89 (July): 102565.
3. Fujita, M., and M. Iwata. 2008. "Reuse System of Building Steel Structures." Structure and Infrastructure Engineering: Maintenance, Management, Life-Cycle Design and Performance 4 (3): 207–20.
4. Mroueh, U. M., P. Eskola, and J. Laine-Ylijoki. 2001. "Life-Cycle Impacts of the Use of Industrial by-Products in Road and Earth Construction." Waste Management 21 (3): 271–77.
5. Lacey, Andrew William, Wensu Chen, Hong Hao, and Kaiming Bi. 2018. "Structural Response of Modular Buildings – An Overview." Journal of Building Engineering 16 (March): 45–56.
6. Hamburger, Ronald O. 2006. "Prequalified Connections for Special and Intermediate Steel Moment Frames for Seismic Applications, ANSI/AISC 358-05." In Structures Congress 2006. Reston, VA: American Society of Civil Engineers. https://doi.org/10.1061/40889(201)5.
7. SAC Joint Venture. Guidelines Development Committee. 2000. Recommended Seismic Evaluation and Upgrade Criteria for Existing Welded Steel Moment-Frame Buildings. Federal Emergency Management Agency.
8. Liu, Xuechun, Xiaojun Zhou, Ailin Zhang, Chen Tian, Xun Zhang, and Yongqiang Tan. 2018. "Design and Compilation of Specifications for a Modular-Prefabricated High-Rise Steel Frame Structure with Diagonal Braces. Part I: Integral Structural Design." Structural Design of Tall and Special Buildings 27 (2): e1415.
9. Cheng, Chin-Tung, and Cheng-Chih Chen. 2005. "Seismic Behavior of Steel Beam and Reinforced Concrete Column Connections." Journal of Constructional Steel Research 61 (5): 587–606.
10. Sherman, D. 1996. "Designing with Structural Tubing." Engineering Journal-American Institute of Steel.
11. Wu, Lai-Yun, Lap-Loi Chung, Sheng-Fu Tsai, Tung-Ju Shen, and Guo-Luen Huang. 2005. "Seismic Behavior of Bolted Beam-to-Column Connections for Concrete Filled Steel Tube." Journal of Constructional Steel Research 61 (10): 1387–1410.
12. Kodur, V. K. R., and D. H. MacKinnon. 1998. "Simplified Design of Concrete-Filled Hollow Structural Steel Columns for Fire Endurance." Journal of Constructional Steel Research 46 (1-3): 298.
13. Azizinamini, Atorod, Yerrapalli Shekar, and M. Ala Saadeghvaziri. 1995. "Design of through Beam Connection Detail for Circular Composite Columns." Engineering Structures 17 (3): 209–13.

14. Elremaily, Ahmed, and Atorod Azizinamini. 2001. “Experimental Behavior of Steel Beam to CFT Column Connections.” Journal of Constructional Steel Research 57 (10): 1099–1119.
15. Mohammadi, S., M. Ghassemieh, and S. R. Mirghaderi. 2020. “Cyclic Behavior of Steel Moment Connections with Built-up Columns in Weak Direction.” Journal of Constructional Steel Research 172 (September): 106224.
16. Mirghaderi, Seyed Rasoul, Shahabeddin Torabian, and Farhad Keshavarzi. 2010. “I-Beam to Box–column Connection by a Vertical Plate Passing through the Column.” Engineering Structures 32 (8): 2034–48.
17. Cao, Shi, Ganping Shu, Kunhong Lin, and Ying Qin. 2018. “Experimental Seismic Behaviour of Bottom-through-Diaphragm and Top-Ring Connection to SST Columns.” Journal of Constructional Steel Research 150 (November): 249–60.
18. Shin, Kyung-Jae, Young-Ju Kim, Young-Suk Oh, and Tae-Sup Moon. 2004. “Behavior of Welded CFT Column to H-Beam Connections with External Stiffeners.” Engineering Structures 26 (13): 1877–87.
19. Ghobadi, M. S., M. Ghassemieh, A. Mazroi, and A. Abolmaali. 2009. “Seismic Performance of Ductile Welded Connections Using T-Stiffener.” Journal of Constructional Steel Research 65 (4): 766–75.
20. Zhang, Ai-Lin, Chuan-Hao Li, Xue-Chun Liu, and Xuesen Chen. 2022. “Seismic Performance of Joint for H-Beam to CFST Column with Field-Bolted Flange-Splicing.” Journal of Constructional Steel Research 196 (September): 107375.
21. Rezaeian, Alireza, Majid Jamal-Omidi, and Farhood Shahidi. 2014. “Seismic Behavior of ConXL Rigid Connection in Box-Columns Not Filled with Concrete.” Journal of Constructional Steel Research 97 (June): 79–104.
22. Yang, Chao, Jun-Fen Yang, Ming-Zhou Su, and Cheng-Zong Liu. 2016. “Numerical Study on Seismic Behaviours of ConXL Biaxial Moment Connection.” Journal of Constructional Steel Research 121 (June): 185–201.
23. Lee, Kyoung-Hyeog. 1998. Boundary Effects in Welded Steel Moment Connection. University of Michigan.
24. Abaqus, G. 2011. “Abaqus 6.11.” Dassault Systemes Simulia Corporation, Providence, RI, USA 3.
25. Selvaraj, Sivaganesh, and Tak-Ming Chan. 2024. “Recommendations for Implementing Circular Economy in Construction: Direct Reuse of Steel Structures.” Journal of Constructional Steel Research 214 (March): 108439.
26. Akbarnezhad, Ali, and Jianzhuang Xiao. 2017. “Estimation and Minimization of Embodied Carbon of Buildings: A Review.” Buildings 7 (1): 5.
27. Engelhardt, Michael D., G. Fry, S. Jones, M. Venti, and S. Holliday. 2000. “Behavior and Design of Radius Cut Reduced Beam Section Connections.” Rep. No. SAC/BD-00 17.